PROCEEDINGS, Thirty-Seventh Workshop on Geothermal Reservoir Engineering
Stanford University, Stanford, California, January 30 - February 1, 2012
SGP-TR-194

MODELLING GEOTHERMAL FLOW AND SILICA DEPOSITION ALONG AN ACTIVE FAULT

David Dempsey, Julie Rowland, and Rosalind Archer

University of Auckland
70 Symonds St
Auckland, 1011, New Zealand
e-mail: d.dempsey@auckland.ac.nz

ABSTRACT

In the Taupo Volcanic Zone (TVZ) of New Zealand geothermal circulation is facilitated high porosity quaternary volcanic deposits, and by fracture permeability associated with widespread normal faulting. High temperature fluids (>250°C) exit the crust at more than 20 locations, many of which are associated with outcropping faults or fault tips, e.g., Te Kopia, Orakeikorako, Waiotapu-Waimangu. Frequent seismicity associated with these structures suggests that fracture permeability is not a static property of the system, but may oscillate or evolve in response to the applied tectonic extension, perhaps modulated by fluctuation in pore fluid pressure. Further, epithermal mineralization in the near surface can have a detrimental effect on permeability, creating a low porosity alteration shroud that influences surface outflow.

In this work we report on a 3-D computational model that considers two perturbations to steady state convection in the vicinity of a fault. First, the rate of mineral deposition, as a function of mass flux and temperature gradient, is used to iteratively update porosity and permeability distributions with time, producing a low permeability capzone and sealing the system. Second, the effects of fault rupture are approximated by a transient permeability increase along a fault plane, permitting renewed circulation to the surface. Results are discussed in the context of geothermal field evolution over geological time scales and effects on the reservoir considered.

INTRODUCTION

In the Taupo Volcanic Zone (TVZ) of New Zealand's Central North Island abundant geothermal circulation and normal faulting coexist. Several geothermal fields are localized on large active faults, frequently at intersections with older structures and at tip zones. Faults are presumed to supply favorable permeability conditions for the transport of hot fluid from depth, operating as a fluid conduit along strike and up-dip.

Development of a silicified capzone above upwelling hydrothermal fluids has been identified in several 'self-sealed' geothermal systems (Facca and Tonani, 1965; Browne, 1978; Dobson et al., 2003). Cooling of hydrothermal fluids saturated with dissolved silica causes precipitation into pore space and sealing of fractures. In systems containing significant amounts of dissolved CO_2 precipitation of carbonates can also play a role in self-sealing.

Fault reactivation affects fluid flow by temporarily fracturing the near fault region and silicified capzone, leading to a transient increase in permeability. These changes are arrested to a degree by enhanced rates of mineralization and fracture sealing that accompany high mass flux rates. Faults may also demonstrate valve-like behavior, by rupturing impermeable barriers hosting overpressured fluids, thereby permitting increased mass flow to the surface (Sibson, 1990).

In this paper we detail a numerical model for geothermal circulation on an active fault. The permeability field evolves continuously in response to silica deposition under a gradient reaction regime (Phillips, 1991). This method has previously been used to model evolving fracture permeability in limestone Karst systems (Chaudhuri et al., 2009). Porosity is modified in response to the silica deposition calculated for a given volume at local temperature gradient and mass flux rates. This corresponds to a permeability increase or decrease in regions of deposition and dissolution, respectively. During fault rupture permeability along the fault plane is reset to its pre-alteration value.

The model demonstrates rapid evolution of a low permeability capzone at the surface, where the vertical temperature gradient, and thus silica

precipitation, is maximum. The capzone causes lateral deflection of rising fluids, resulting in a steady widening of both field area and capzone dimension. Fluids below the capzone increase in temperature and enthalpy due to the insulating properties of the low porosity/permeability rock above. Fault rupture causes a substantial increase in heat output through the field as fluids ascend directly to the surface. However, this increase is transient and resealing of the fault returns the system to its pre-earthquake state.

NUMERICAL MODEL

Geothermal circulation is modeled using the Finite Element Heat and Mass transfer (FEHM) code (Zyvoloski et al., 1988). A model domain with dimensions 15×15 km in the horizontal plane, and 8 km in the vertical direction, is partitioned into ≈185 000 elements, with a higher density at the surface and within a central fault plane (see Figure 1). This ensures temperature gradients are well resolved in regions where the greatest permeability modification is expected.

Convection is driven by an applied temperature boundary condition at the base of the model. A Gaussian temperature distribution, with maximum value 340°C, ensures the upflow zone is localized in the center of the model domain. This corresponds to the approximate temperature of the brittle-ductile transition (Sibson, 1977), and the inferred limit of fracture permeability. The domain depth of 8 km is consistent with seismic data suggesting this is the lower limit of the brittle crust (Bryan et al., 1999)

Atmospheric temperature (20°C) and pressure (100 kPa) boundary conditions are maintained at the upper surface of the model. All model boundaries are closed to mass flux, and plume recharge is supplied by downward percolation of cold fluid outside the central upflow zone.

Permeability modification by silica deposition

The distance over which disequilibrium with respect to dissolved silica prevails determines the type of reaction regime under consideration. For high fluid velocities and low reaction rates, disequilibrium prevails over long distances and consideration of reactions kinetics is necessary to provide a numerical description of circulation. However, in geothermal systems, mass flux rates are typically low, which provides sufficient time for dissolved silica concentrations to equilibrate to the local solubility. Deposition and dissolution can then be described in terms of the gradient in silica solubility, which itself is a function of some controlling variable, typically temperature. Mass flow, **M**, perpendicular to the temperature gradient, ∇T, is isothermal and therefore does not participate in deposition or dissolution. Discussion of mass flux here refers to that component parallel to ∇T.

Consider the transport of fluid through some volume element, across which the temperature changes by an amount ΔT. As silica solubility, m_q, depends primarily on temperature (Fournier and Potter, 1982), the consequent change in m_q is given by

$$\Delta m_q = \frac{dm_q}{dT}\Delta T. \qquad (1)$$

Accounting for the rate of mass transport through a volume element over some time, Δt, the change in porosity, $\Delta\phi$, due to deposition or dissolution of solid

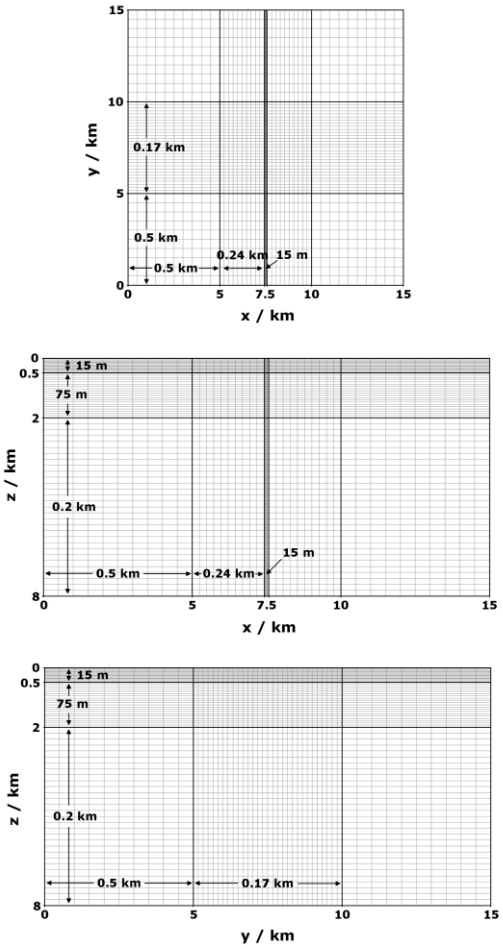

Figure 1: Mesh dimensions. Arrows indicate extent over which nodal spacings apply, e.g., for x between 0 and 5 km the nodal spacing is 0.5 km. Note that the unmarked fault width is 150 m and this has been partitioned into 10 layers.

quartz is given by

$$\Delta\phi = \int_{t_0}^{t_0+\Delta t} \boldsymbol{M}(t) \cdot \nabla T(t) \frac{dm_q}{dT} \frac{M_q^{mol}}{\rho_q} dt, \qquad (2)$$

where M_q^{mol} is the molar mass and ρ_q the density of precipitated quartz. This equation determines silica deposition by changes in temperature, but does not account for boiling or changes in pH.

Permeability modification in FEHM

Silica modification of the porosity and permeability distributions is implemented through an iterative update scheme. Geothermal circulation is simulated for a nominal time period of 500 years with mass flux and temperature fields output at ten evenly spaced time steps. For each time step, a change in porosity is calculated according to Eq. (2) with Δt the time step length, and **M** and ∇T interpolated at the midpoint of the time step. The total porosity change for the ten time steps modifies the porosity and permeability distributions in FEHM, and the simulation is restarted for another 500 yr. Temperature and pressure fields at the end of each simulation are used as initial conditions for the simulation restart.

After a period of 20 kyr, i.e., forty 500 yr simulations, the update period is increased by a factor of 10 to investigate long term silica deposition. This typically occurs in the deeper crust where temperature gradients, and thus alteration rates, are lower.

To describe the effects of silica deposition on fluid flow we require a functional relationship between permeability, k, and porosity, ϕ. We divide the crust into two domains, based on its inferred structure, and a different relationship is prescribed for each. The upper 2 km of the TVZ is characterized by high porosity volcanic deposits. In this domain we expect permeability to be dominated by connected pore space, which above some critical porosity, ϕ_c, follows a $k \propto \phi^3$ relationship (Zhang et al., 1994). Below the critical porosity, 4% in simulations presented here, permeability reduction accelerates and we have chosen a quadratic relationship to describe this region. The minimum obtainable permeability is 10^{-16} m^2 at a porosity of 2%. While this does not represent completely impermeable rock, we propose this represents a plausible minimum value in a region of: (i) ongoing tectonic fracturing, and (ii) hydro fracturing induced by over pressurization at reduced permeability.

At depths greater than 2 km the crust is characterized by homogeneous basement rock (greywacke). In this domain permeability is maintained by networks of interconnecting fractures, which themselves are maintained by high rates of tectonic extension (Wallace et al., 2004). Studies of fractured oil reservoirs (Leary and Al-Kindy, 2002) indicate that under these conditions porosity has a logarithmic dependence on permeability, i.e., $\phi \propto \log(k)$.

The effects of pore compaction and fracture closure, in the upper and lower domains respectively, are approximated by an initial permeability distribution

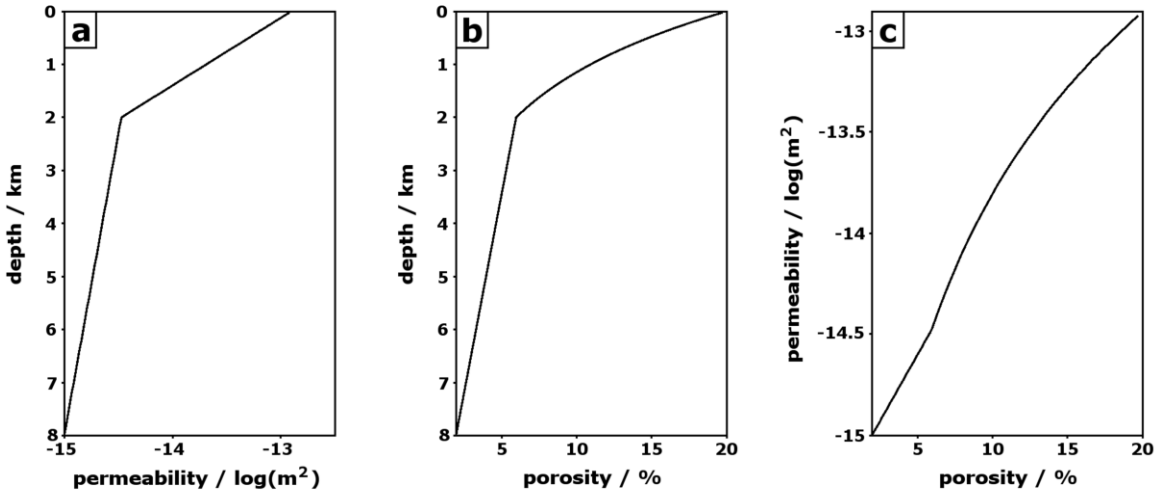

Figure 2: (a) Initial permeability and (b) porosity distributions with depth. The discontinuity at 2 km depth represents the transition from porous permeability to fracture permeability. (c) Relationship between permeability and porosity.

that decreases exponentially with depth (Saar and Manga, 2004). Porosity, permeability and depth relationships are shown in Figure 2.

Seismic cycling of permeability

Circulation is modeled on a mesh containing a high density of nodes through a central, vertical fault plane. This allows fine scale adjustment to fault permeability without influencing the host rock. We assume that fault reactivation permanently increases permeability on the fault through the creation or reshearing of existing fractures. In FEHM, this is implemented by resetting permeability on fault nodes to their original values and superimposing on this a random, spatially correlated fluctuation field.

After 120 kyr of permeability alteration (i.e., forty 500 yr followed by twenty 5000 yr simulations), a fault rupture is prescribed and the simulation length reduced: first to 50 yr for twenty simulations, then increased to 500 yr for another twenty simulations. This allows us to observe fluid flow and permeability alteration at short timescales in the period immediately following an earthquake.

FORMATION OF A CAPZONE

At t = 0 fluid in the model domain is a uniform, cool 20°C. Application of the Gaussian temperature boundary condition at the base of the model develops a stable convective plume after a period of 150 kyr. The upflow zone forms at the center of the model domain above the maximum basal temperature, and recharge occurs along the flanks of the plume. Maximum temperatures in the subsurface (z = 250 m) are approximately 200°C (Figure 3(a)). The geothermal field boundary at the surface, as delineated by the 1 Wm^{-2} vertical heat flux contour, constrains an area of 1.2 km^2, which is somewhat smaller than TVZ fields. However, the model does not account for hydrological surface processes that can increase field area, e.g., lateral subsurface flows. Heat output through the field boundary is 69 MW which is consistent with a medium sized TVZ geothermal field.

Permeability modification by deposition and dissolution of silica commences at t = 200 kyr, at the short update period of 500 yr. For the first 20 kyr alteration rates are the greatest in the top layer of the model due to the high temperature gradients prevailing here. Hot, buoyant fluids ascending within the plume encounter cool meteoric waters at the surface and a boundary layer is formed. As mass flux and temperature gradient are approximately parallel (vertical) deposition of silica and reduction of porosity proceeds rapidly. The consequent effect on permeability (Figure 2(c)) leads to the formation of a low permeability capzone at the surface (Figure 3(d)). Mass flux vectors, which were approximately vertical prior to alteration, are steadily rotated into the horizontal direction as vertical flow is reduced. Lateral deflection of the hot geothermal fluids (Figure 3(d)) shifts the maximum alteration rates to the margins of the capzone, thereby increasing its horizontal extent.

Second order modification of the permeability field is apparent at longer timescales, i.e., for permeability update at 5 kyr intervals. At this stage permeability in the capzone has reached a minimum value of 10^{-16} m^2, however it continues to thicken to a depth of 100-200 m, and also increase in horizontal extent. The relatively slow rate of vertical thickening, relative to horizontal widening, is due to the absence of a boundary layer beneath the cap. Although not modelled here, deposition of silica would proceed

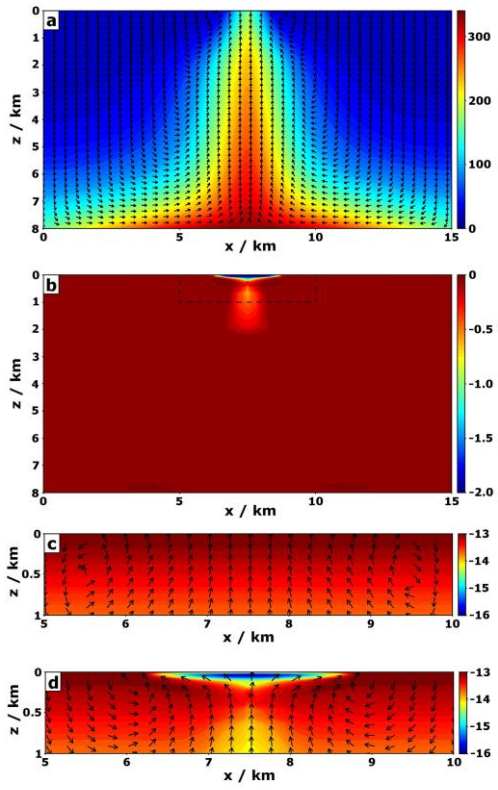

Figure 3: (a) Pre alteration (t = 200 kyr) temperature distribution with mass flux direction vectors. (b) Change in permeability following 120 kyr of silica alteration. Dashed line indicates the limits of (c) pre-alteration permeability distribution and (d) post-alteration permeability distribution. Mass flux direction vectors have been superimposed on (c) and (d).

more rapidly in this region if cool inflows of surface water, perhaps driven by local topography, were present.

Silica deposition and permeability modification also occurs along the axis of upflow to great depths. A wide (~1 km) deposition zone occurs at depths of 1-2 km within the porous volcanic deposits, reducing permeability here by more than half an order of magnitude (Figure 3(b)). Deeper, in the fractured greywacke, permeability reduction occurs at an even slower rate.

We also note a conspicuous absence of permeability modification from large regions of the model. For example, considerable horizontal temperature gradients exist between regions of upflow (250-300°C) and downflow (20-50°C). However, due to vertically oriented mass flows in these regions **M** and ΔT in Eq. (2) are nearly perpendicular, and therefore flow is mostly isothermal. Permeability modification in regions of downflow is also absent due to relatively low temperature gradients. Silica dissolution may proceed at appreciable rates at the base of the brittle crust where a second boundary layer between cold recharging fluids and hot magmatic conduction is formed. However, due to mesh coarseness in this region we are unable to resolve this effect.

Evolution at two different timescales

Figure 4 plots the evolution of several field properties at three different depths over the short and long time scales investigated here. The formation and widening of an impermeable capzone at the surface, which has a limited influence on circulation with increasing depth, has significant consequences for field properties at the surface, i.e., heat output, area and temperature properties. For the purposes of comparison, heat output (Figure 4(a) and (e)), mean permeability ((c) and (g)) and maximum temperature ((d) and (h)) are calculated based on the original field dimensions for the given depth. Field area (Figure 4(b) and (f)), as defined by the 1 Wm^{-2} vertical heat flux contour, changes with time and is thus not directly comparable to the other plots. Total field heat output within the evolving field boundary is given by the black dashed lines in Figure 4(a) and (e).

Figure 4(c) shows that the initial permeability decline in the capzone is substantial and occurs at a constant rate. Some reduction in dk/dt is observed after 10 kyr, which indicates reduced flow through the surface is beginning to exercise a negative feedback on the capzone. By comparison, permeability alteration below the cap (at 100 and 200 m) does not operate on these short timescales due to low temperature gradients.

The decline in surface permeability as the capzone forms affects the thermal properties of the field. For instance, vertical heat flux through the original field boundary drops rapidly in response to the reduced mass flow. Effects on heat flow beneath the capzone are less significant and indicate that the upflow zone is being masked rather than quenched. The discrepancy in vertical heat flow between 25 and 200 m depth indicates the presence of lateral heat flows. Alternatively, where there is a deficit between lateral heat flows and vertical throughput, reservoir heat content may be changing.

Decreasing heat flow in the region above the main upflow zone suggests the capzone plays an insulating role to the flow beneath. This inference is borne out in temperature profiles (Figure 4(d)), which show a steady, if small, increase over the 20 kyr period. However, despite an attendant increase in fluid enthalpy, reduced mass flow below the cap ensures that vertical heat flux decreases (Figure 4(e)).

An interesting feature of the short term surface temperature is the lag between the onset of permeability alteration and the thermal response of the field. Despite a steady decline in surface permeability between t = 200 and 210 kyr, the maximum temperature in this layer records a small increase. However, at t = 210 kyr a slow decrease is observed, which reflects conductive heat loss to the atmosphere outstripping advective heating of rising fluids.

Over longer time periods the negative feedbacks and stabilizing behavior of surface silica deposition are evident. Permeability decline within the capzone, which showed signs of arrest at short timescales (Figure 4(c)), hyperbolically approaches the minimum permeability of 10^{-16} m^2. Permeability decline due to slower rates of silica deposition is also evident at 100 m depth at this time. Arresting decline in the surface permeability properties is matched by a similar decline in vertical heat flux through the original field boundary. However, this does not correspond to an overall reduction in field output. Rather, a constant output of 60 MW is distributed over an increasing field area (Figure 4(f)).

Field area, as constrained by the 1 Wm^{-2} vertical heat flux contour, increases at a steady rate of approximately 2.7 km^2 per 100 kyr as deposition of silica at the surface proceeds. The data indicate that within the top 200 m the plume widens with increasing proximity to the surface. Deeper in the

crust the opposite trend is inferred to prevail, as a decreasing mass flux (due to decreasing permeability) is accommodated across a wider area (Bibby et al., 1995).

EFFECTS OF FAULT RUPTURE

The effects of fault rupture to the surface are approximated by a step change in permeability along the fault plane. Nodes contained within the 150 m wide fault zone (Figure 1) are reset to their original, pre-alteration permeability values. This restores fluid flow through the center of the capzone and considerably perturbs the heat flow characteristics of the field.

Perhaps the most significant effect of fault rupture is the immediate increase in heat output at the surface (Figure 5(a)). Total field output increases by approximately 50% from the original 60 MW to more than 90 MW. This is due to the increased fluid throughput and is accompanied by the restoration of pre-alteration surface temperatures of ~150°C as ascending fluids heat the atmospherically cooled capzone.

Silica deposition at the surface proceeds rapidly in the period following fault rupture. This is due to the increased mass flow rates and vertical temperature

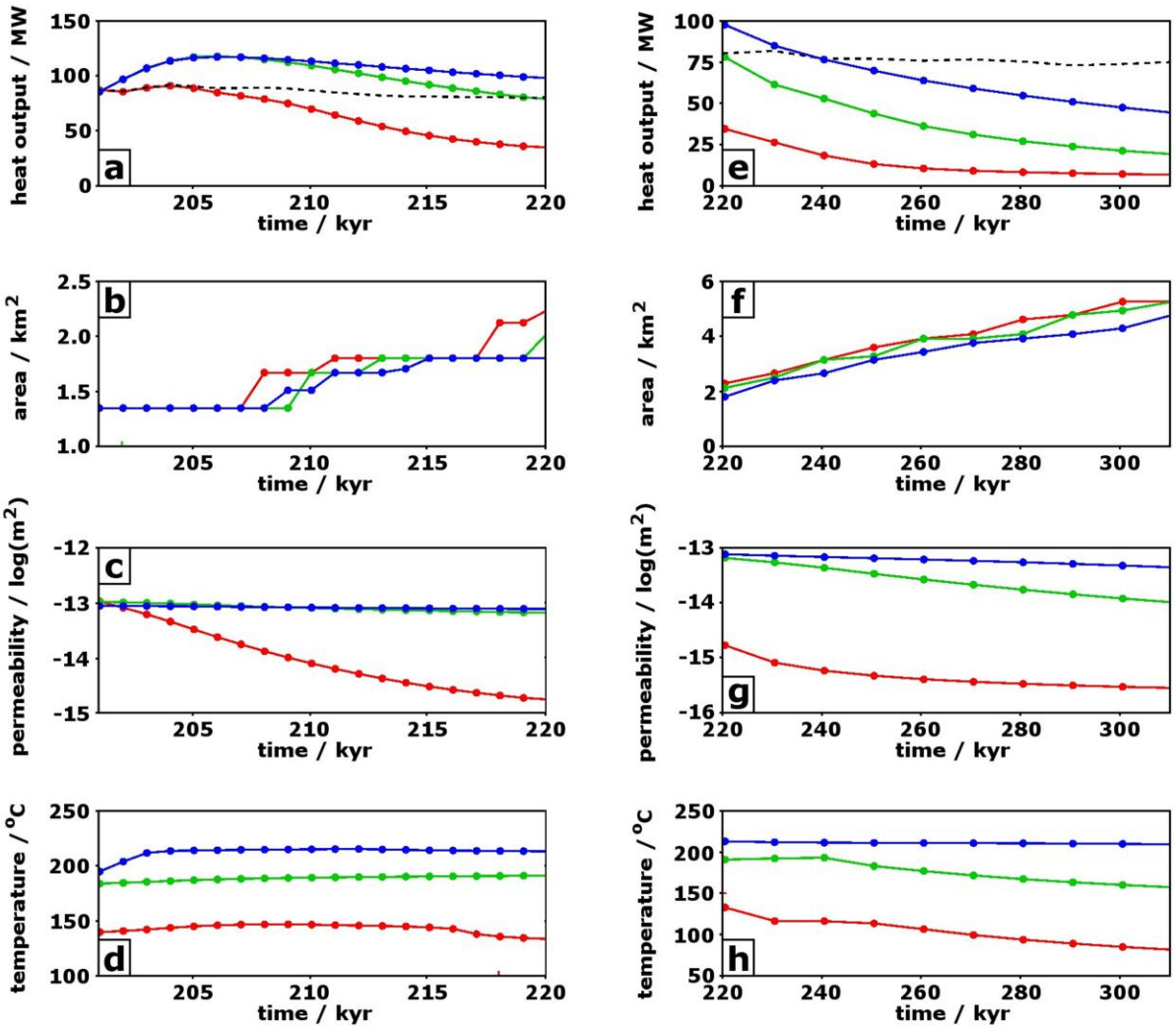

Figure 4: Evolution of geothermal field properties at three different depths: 25 (red), 100 (green) and 200 m (blue). Changes in (a) vertical heat flow, (b) field area, (c) mean permeability, and (d) maximum temperature are shown over a period 20 kyr, for the short update period of 500 yr. Quantities in (a), (c) and (d) are measured for the original field boundary. Changes in these properties are also shown in (e-h) over a period of 90 kyr, for the longer update period of 5000 kyr. Black dashed line in (a) and (e) indicates total field output calculated based on the expanding field area.

gradient. Within 1-2 kyr heat output is restored to the original 60 MW via resealing of the fault zone. Once again, we observe a lag in surface temperature reduction from atmospheric cooling.

LATERAL HEAT DEFLECTION

Figure 6 shows evolving vertical and lateral heat flows in the near surface upflow zone of the geothermal system. Prior to development of a self-sealing cap heat throughput is largely vertical (Figure 6(b) and (c)) and confined to a zone ~1 km wide in the centre of the model. Small, positive lateral flows at this time represent entrainment of fluid into the plume as permeability decreases with depth.

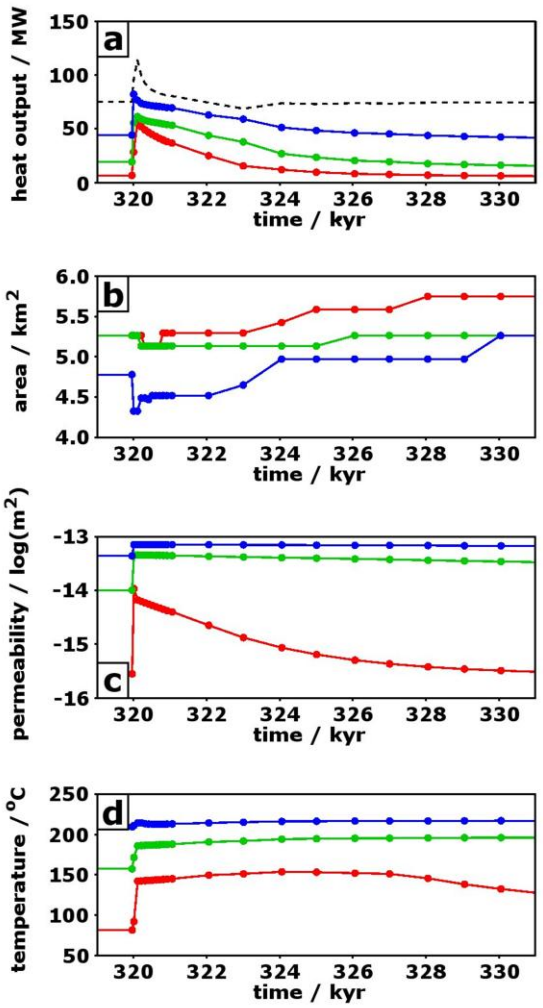

Figure 5: Evolution of geothermal field properties for the period following fault rupture (t = 320 kyr) at depths of 25 (red), 100 (green), and 200 m (blue).(a) Heat output, (b) field area, (c) mean permeability, and (d) maximum temperature are shown. The black dashed line in (a) indicates total field output.

Ongoing self-sealing of the geothermal system results in significant lateral deflection of rising fluids. Figure 6(a) shows that for a thickened capzone, these flows occur between 50 and 400 m depth, with a peak at ~200 m. The close match between across and along strike lateral flows indicates this deflection is largely symmetrical. Vertical heat flow at the surface has been reduced to about 85-90% of its pre-alteration value. However, at a depth of 1 km the reduction is only 20%.

Differences in along and across strike heat transfer are evident following fault rupture. Lateral heat flows are immediately halved as vertical flow pathways to the surface are restored. Further, along strike lateral flows appear to migrate closer to the surface into newly created capzone permeability. Figure 6(b) shows that heat flux at the surface is characterized by renewed flow along the fault trace, which now bisects the otherwise impermeable capzone. Heat flux at depth (Figure 6(c)) also increases to accommodate the increased field output.

Silica deposition in the near surface in the post-seismic period results in a return to the pre-seismic flow regime. Across strike lateral flow recovers to its original value, however along strike flow, taking advantage of new fault permeability, is more vigorous and shallower than before. Surface heat flux returns to its pre-seismic minimum and the field is once again masked by the presence of a contiguous silicified cap.

RESERVOIR RESPONSE

By delineating a hypothetical geothermal reservoir in the main upflow zone, we can qualitatively describe the effects of capzone formation and fault rupture on the heat content of the resource. As a first approximation, and because the capzone evolves a circular shape, we select a cylindrical surface to constrain the reservoir. The surface has a diameter of 2 km, extends to a depth of 2 km representing readily

Table 1: Reservoir heat content during simulation.

Time (kyr)	Simulation stage	Reservoir energy (EJ)
201	pre-alteration	2.75
320	pre-earthquake	3.36
320.5	minimum post-earthquake	3.25
330	maximum recovery	3.35

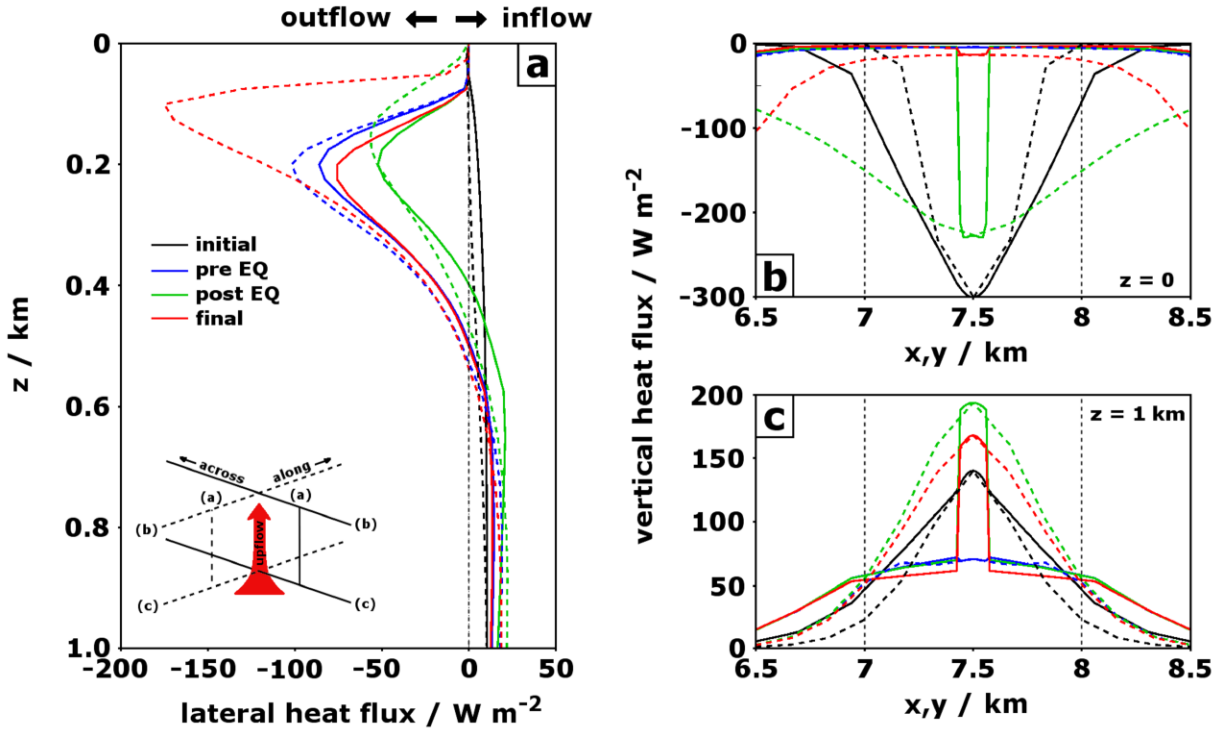

Figure 6: Heat flow profiles across hypothetical boundaries constraining the central upflow zone. (a) Lateral across (solid) and along (dashed) strike heat flows at a radial distance of 500 m from the upflow axis (x = y = 7.5 km). (b) Vertical heat flux across a horizontal transect at the surface (z = 0), and (c) at 1 km depth. Dashed lines in (b) and (c) indicate the positions of the observation planes inset in (a). Colors show heat flow at four different stages: prior to capzone formation (black, t = 200 kyr), after formation of a capzone and prior to fault rupture (blue, t = 309 kyr), immediately following fault rupture (green, t = 320 kyr), and after fault resealing (red, t = 330 kyr). Note that positive heat flows represent heat entering the observation planes inset in (a).

accessible drilling depths in the TVZ. The reservoir is situated in the centre of the model along the main upflow axis. Table 1 shows reservoir heat content in Exajoules (1 EJ = 10^{18} J) at four different stages during the simulation.

A large increase in reservoir energy occurs during the 120 kyr period of alteration preceding fault rupture. This is due to a broadening plume beneath the developing capzone, resulting in higher temperatures and enthalpies within the reservoir. Rapid mass flow accompanying fault rupture causes a steady depletion of reservoir heat content. This decline is eventually arrested by mineralization within fractures in the fault zone, but this is not achieved until ~500 years after the rupture. Insulation of the convective cell and recovery of enthalpy over the following 10 kyr restores the reservoir heat content to its pre-rupture value.

CONCLUSION

A numerical model has been described that accounts for porosity changes due to silica deposition under a gradient reaction regime. Subsequent changes in the permeability field permit the investigation of the negative feedback that mineralization exerts on hydrothermal flow. An impermeable capzone develops above the upflow zone, resulting in:

(i) Increasing reservoir heat content through insulation from the atmosphere.
(ii) Increasing field area through lateral deflection of rising fluids.
(iii) Masking of field presence through a decreased surface heat flux.

The effects of fault rupture through the capzone, and subsequent mineral sealing, have also been investigated. Restoration of fault permeability results in increased surface heat flux along the fault trace and an increase in total field output. Lateral flows are initially decreased but recover during the post-rupture period as the capzone reseals. A small depletion of

the geothermal reservoir is also observed, however this is arrested after 500 yr and recovery of the pre-earthquake reservoir is achieved after 10 kyr.

REFERENCES

Browne, P. R. L. (1978), "Hydrothermal alteration in active geothermal fields," *Annual Review of Earth and Planetary Sciences*, **6**, 229-250.

Bryan, C. J., Sherburn, S., Bibby, H. M., Bannister, S. C. and Hurst, A. W. (1999), "Shallow seismicity of the central Taupo Volcanic Zone, New Zealand: its distribution and nature," *New Zealand Journal of Geology and Geophysics*, **42**, 533-542.

Chaudhuri, A., Rajaram, H., Viswanathan, H., Zyvoloski, G. and Stauffer, P. (2009), "Buoyant convection resulting from dissolution and permeability growth in vertical limestone fractures," *Geophysical Research Letters*, **36**, doi: 10.1029/2008GL036533.

Dobson, P. F., Kneafsey, T. J., Hulen, J. and Simmons, A. (2003), "Porosity, permeability, and fluid flow in the Yellowstone geothermal system, Wyoming," *Journal of Volcanology and Geothermal Research*, **123**, 313-324.

Facca, G. and Tonani, F. (1965), "The Self-sealing Geothermal Field," *Proceedings of the IAV International Symposium on Volcanology (New Zealand)*, 271-273.

Fournier, R. O. and Potter, R. W. (1982), "An equation correlating the solubility of quartz in water from 25° to 900°C at pressures up to 10,000 bars," *Geochimica et Cosmochimica Acta*, **46**, 1969-1973.

Leary, P. C. and Al-Kindy, F. (2002), "Power-law scaling of spatially correlated porosity and log(permeability) sequences from north-central North Sea Brae oilfield well core," *Geophysical Journal International*, **148**, 426-442.

Phillips, O. M. (1991), "Flow and Reactions in Permeable Rocks," *Cambridge University Press*, U. K.

Saar, M. O. and Manga, M. (2004), "Depth dependence of permeability in the Oregon Cascades inferred from hydrogeologic, thermal, seismic, and magmatic modeling constraints," *Journal of Geophysical Research*, **109**, doi: 10.1029/2003JB002855.

Sibson, R. H. (1977), "Fault rocks and fault mechanisms," *Journal of the Geological Society of London*, **133**, 191-213.

Sibson, R. H. (1990), "Conditions for fault-valve behaviour," In: Knipe, R. J., and Rutter, E. H. (eds), Deformation Mechanisms, Rheology and Tectonics, *Geological Society of London Special Publications*, **54**, 15-28.

Wallace, L. M., Beavan, J., McCaffrey, R. and Darby, D. (2004), "Subduction zone coupling and tectonic block rotations in the North Island, New Zealand," *Journal of Geophysical Research*, **109**, doi: 10.1029/2004JB003241.

Zhang, S., Paterson, M. S. and Cox, S. F. (1994), "Porosity and permeability evolution during hot isostatic pressing of calcite aggregates," *Journal of Geophysical Research*, **99**, 15,741-15,760.

Zyvoloski, G. A., Dash, Z. V. and Kelkar, S. (1988), "FEHM: Finite element heat and mass transfer code," *Report LA-11224-MS*, Los Alamos National Labs, Los Alamos, NM.